Generation of bonding and antibonding photonic modes in laser-induced photonic double quantum wells

S. M. Sadeghi*
Department of Physics, University of Alabama in Huntsville, Huntsville, Alabama 35899, USA

W. Li
Department of Chemistry and Engineering Physics, University of Wisconsin–Platteville, Platteville, Wisconsin 53818, USA

(Received 23 January 2010; revised manuscript received 11 March 2010; published 21 April 2010)

We study generation of photonic modes, including bonding and antibonding modes, in a laser-induced photonic double quantum well. Such a quantum well is formed via illumination of a special type of a photonic waveguide structure (photonic superstructure) with a laser field. Striking similarities between states of electrons in electronic double quantum wells and photonic modes in symmetric and asymmetric photonic double quantum wells are predicted. We show that in such photonic quantum wells one can use the laser field to control the degree of mixing of the bonding and antibonding photonic modes (subbands), forming pure to strongly mixed transmission states.

DOI: 10.1103/PhysRevB.81.155317 PACS number(s): 42.70.Qs, 78.67.De, 42.50.−p

Formation of photonic modes similar to confined-electronic states in semiconductor nanostructures is an appealing subject of research with many fundamental and practical applications. In some respect such research is motivated by the fact that spatial confinement of electrons in semiconductor systems has led to many useful and interesting phenomena. These phenomena are related to the fact that in confined electronic structures, such as quantum wells (QWs), quantum dots, quantum wires, and superlattices, one can tailor the electronic band structures of semiconductors to a large extent. Significant research has been carried out to confine photons in similar ways. It has been shown that by decreasing the lateral size of a photonic quantum dot, one can shift the optical modes to higher energies.[1–4] These modes are analogous to sharp discrete states of an electronic quantum dot.[5,6] Additionally by bringing two or more of photonic cavities together one can even form a "photonic molecule," generating bonding and antibonding modes.[7–10] It was also shown that, similar to semiconductor QW structures, one can use different photonic band gaps (PBGs) to construct photonic QW structures, provided the band gaps of the constituent PBGs are aligned properly.[11,12]

In a recent paper we studied a special type of photonic waveguide structure called photonic superstructure.[13] In the absence of a laser field (control field) this structure acted as a passive PBG structure. When a region of this structure was illuminated by the control field, the index perturbation in that region was either increased or decreased, forming a photonic heterostructure.[13] Such photonic superstructures can be used for generation of photonic QWs with either valencelike or conductionlike bands and have device applications such as time-delay lines.[13,14] Our objective in this paper is to study generation of bonding and antibonding photonic modes using a photonic superstructure. For this we explore the striking similarities between electronic subbands in semiconductor double quantum wells (S-DQWs) and photonic subbands (PSB) in the photonic double quantum wells (P-DQWs) formed using such a structure (Fig. 1). We show that using a single photonic superstructure one not only can generate symmetric and asymmetric P-DQWs with photonic subbands (modes) very similar to those of their electronic counterparts but also can have control over the degree of mixing of the bonding and antibonding photonic modes. Therefore, instead of static variation in the structural parameters, as those in photonic molecules formed by microcavities, here by changing the illumination geometry and/or intensity of the control field we can make different photonic systems with controllable mixed modes. These processes happen via utilization of

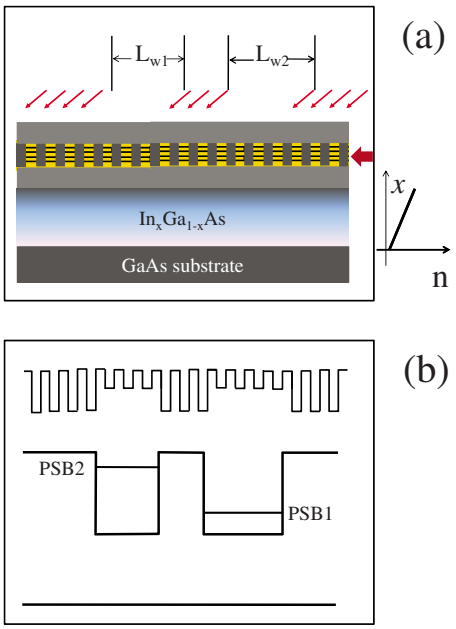

FIG. 1. (Color online) (a) Structural details and illumination geometry of the photonic superstructure. (b) Variation in refractive index (top) and photonic band gap (down) along the propagation direction. PSB1 and PSB2 refer to the photonic subbands (resonant transmission states) and the horizontal arrows in (a) represent the control field. The diagram to the right of (a) shows variation in refractive index of the buffer layer along the growth direction (z). The thick horizontal arrow in (a) refers to the signal beam.

 ©2010 The American Physical Society

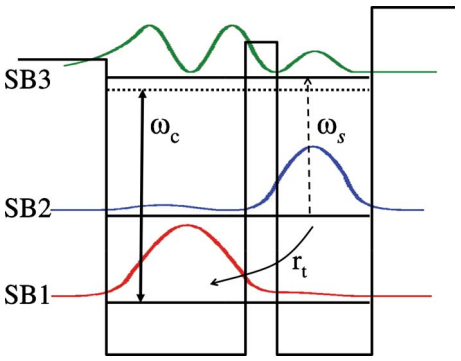

FIG. 2. (Color online) Schematic illustration of the S-DQW conduction band structure. ω_s and ω_c refer, respectively, to the signal and control field frequencies. The energies of the SB1-SB3 and SB2-SB3 transitions are, respectively, 391 and 239 meV. r_t represents the tunneling rate.

coherent processes such as electromagnetically induced transparency (EIT) and resonant suppression of refractive index formed in the intersubband transitions of a S-DQW.

In this study we consider an n-doped S-DQW structure consisting of 4 and 2 nm $In_{0.5}Ga_{0.5}As$ wells separated by 1.5 nm $Al_{0.5}Ga_{0.5}As$ barrier (Fig. 2). The left and right barriers are, respectively, $Al_{0.4}Ga_{0.6}As$ and $Al_{0.55}Ga_{0.45}As$. The conduction band of such a structure, as shown in Fig. 2, supports three conduction subbands: $|1\rangle$ (SB1), $|2\rangle$ (SB2), and $|3\rangle$ (SB3). Including the effects of strain and energy-dependent electron effective mass, we found a relatively large dipole moment for the 2-3 transition ($\mu_{23}=2.7e\times$ nm) with a transition wavelength of about 5.2 μm. The 1-3 transition occurs at 3.17 μm with $\mu_{13}=0.8e\times$ nm. We considered the electron-electron scattering rate in the ground subband was 4 ps^{-1} and the energy relaxation times of electrons from the third subband to the second and first subbands were, respectively, 2 and 3 ps.[13] In addition, considering the 1-2 transition energy (152 meV) and the QW carrier density (7×10^{11} cm^{-2}), we assumed the tunneling time from $|2\rangle$ to $|1\rangle(1/r_t)$ was roughly 2.5 ps. We considered the control field with frequency ω_c and intensity I was near resonant with the 1-3 transitions while the signal or probe field with frequency ω_s detected the 2-3 transitions (Fig. 2).

The optical response of the S-DQW in the vicinity of the 2-3 transition was calculated using the optical Bloch equations.[13,14] Figure 3 shows (a) absorption coefficient and (b) refractive index of the 2-3 transition within a frequency range around the Bragg wavelength of the PBG. It is clear that in the absence of the control field the 2-3 transition is basically transparent with a refractive index equal to that of the background index of the S-DQW structure (n_b) (Fig. 3, dashed lines). In the presence of this field the absorption coefficient and refractive index of this transition changes dramatically. In particular, if we consider the intensity of this field (I) is 0.7 MW/cm^2 and its wavelength is 3.2 μm, as shown in Fig. 3(a), around 5.13 μm an EIT is generated (downward arrow). Considering Fig. 3(b), around the same wavelength one finds significant suppression of refractive index. EIT is a process where the absorption of a transition is coherently suppressed although the upper state of that transition is nearly empty.[15] Similar to EIT, the refractive index change is also caused by coherent process involving interference between transitions from SB2 to SB3 (the 2-3 transition) and from SB2 to SB1 via SB3 (the indirect 2-3-1 transition).

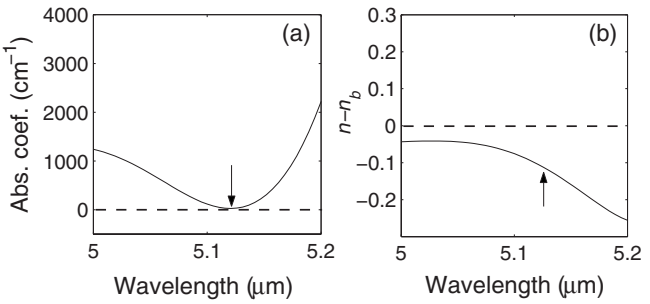

FIG. 3. (a) Absorption coefficient and (b) refractive index of the 2-3 transitions when the intensity of the control field is 0.7 MW/cm^2 and its detuning is 4.1 meV. The downward arrow in (a) indicates the wavelength where EIT occurs and that in (b) shows suppression of refractive index at the same wavelength. The dashed lines refer to the case when the control field is off.

To study the impact of refractive index and absorption changes on the light scattering along the waveguide shown in Fig. 1, we assumed it was consisted of 80 periods of the S-DQW grown on the top of the lower cladding layer. These QWs were then all etched periodically with $\Lambda=813$ nm and 50% duty cycles (Λ is the period of the corrugation). The trenches were then refilled epitaxially with $In_xAl_{1-x}As$. The In content (x) here was adjusted such that the effective refractive indexes of these regions (trenches) were more than those of the QW regions in the absence of the control field. The substrate is GaAs and the lower buffer layer was considered to be a graded $In_xAl_{1-x}As$ layer. This layer not only allows accommodation of high strain but also it provides the optical confinement needed for the waveguide structure by gradual increase in the refractive index [diagram to the right of Fig. 1(a)]. The upper confinement layer was also taken to be $In_xAl_{1-x}As$ with an average refractive index of 3 in the vicinity of 5 μm, similar to that of the lower confinement layer. The length of total waveguide (L_t) was considered to be about 1400 μm and the facets are antireflection coated. We also assumed the S-DQWs were located a narrow-width ridge illuminated from the side by the control field. This allows us to ignore variation in the control field intensity.[16]

To study light scattering along the waveguide structure, note that the absorption coefficient (α) and refractive index change ($\Delta n=n-n_b$) shown in Fig. 3 determine the dielectric function of the S-DQW structure according to the following:

$$\Delta\varepsilon^{\mathrm{QW}}_{\omega_c,I}(\omega_s)=2n_b\Delta n(\omega_s)-j\frac{n_bc}{\omega_s}\alpha(\omega_s). \quad (1)$$

Therefore, considering the periodicity of the S-DQW structure along the propagation axis (z), for the waveguide structure we have

$$\varepsilon_{\omega_c,I}(\omega_s,r,z)=\varepsilon_0+\Delta\varepsilon^{\mathrm{bg}}(r,z)+\Delta\varepsilon^{\mathrm{QW}}_{\omega_c,I}(\omega_s,r,z). \quad (2)$$

Here ε_0 is related to the effective refractive index of the waveguide in the absence of the QW corrugation and

$\Delta\varepsilon^{\mathrm{bg}}(r,z)$ represents the contrast of the background refractive indices of the QW and trench regions in the absence of the control field. $r \equiv (x,y)$ refers to the cross-sectional position of the waveguide. Note that in Eq. (2) $\Delta\varepsilon^{\mathrm{QW}}_{\omega_c,I}(\omega_s,r,z)$ is equal to $\Delta\varepsilon^{\mathrm{QW}}_{\omega,I}(\omega_s)$ in the QW regions and zero elsewhere. In Eq. (1) c refers to the speed of light.

The slowly varying part of the light wave along the waveguide structure considered here can be expressed as

$$E^I_{\omega_c}(\omega_s,z) = F^I_{\omega_c}(\omega_s,z)e^{-j\beta_0 z} + R^I_{\omega_c}(\omega_s,z)e^{j\beta_0 z}. \quad (3)$$

Here the indices emphasize on the fact that the optical-field propagation along the functional waveguide structure considered in this paper is strongly influenced by the intensity (I) and frequency (ω_c) of the control field. For the first-order corrugation with period Λ considered here we have $\beta_0 = \pi/\Lambda$. $F^I_{\omega_c}(\omega_s,z)$ and $R^I_{\omega_c}(\omega_s,z)$ refer to the forward and backward waves with frequency ω along z. To find these functions we adopted a transfer-matrix method. The details of calculations are presented in Refs. 13 and 16.

To have a P-DQW, we need to consider the control laser illuminates three regions of the waveguide, forming two barriers at the side and one at the middle (Fig. 1). The widths of these barriers can be changed by varying the widths of the illuminated regions. In the following L_{mb} represents the middle barrier width, and L_{w1} and L_{w2} refer, respectively, to the widths of the left and right wells (Fig. 1). We consider the intensity of the control field is 0.7 $\mathrm{MW/cm^2}$ and its detuning from the 1-3 transition is 4.1 meV, as those in Fig. 3. As shown in Fig. 4(a), the results show that when $L_{\mathrm{w1}}=250$, $L_{\mathrm{w2}}=200$, and $L_{\mathrm{mb}}=300$ μm, i.e., having an asymmetric P-DQW, the transmission spectrum of the structure shows two narrow transmission lines close to each other inside the band gap. Figures 4(b) and 4(c) show the corresponding squared longitudinal profiles ($|F^I_{\omega_c}+R^I_{\omega_c}|^2$) associated with these modes. The results show significant similarities with the envelope functions of the conduction subbands of conventional asymmetric S-DQW structures (Fig. 2). Here Fig. 4(b) represents the lower energy mode (PBS1), wherein interestingly the mode is mostly located in the wider well (L_{w1}). Accordingly, in the case of Fig. 4(c) the higher energy mode (PBS2) now mostly resides in the narrower well (L_{w2}).

The results of calculations when the $L_{\mathrm{w1}}=L_{\mathrm{w2}}=200$ μm (symmetric P-DQW) and $L_{\mathrm{mb}}=300$ and 100 μm are shown in Fig. 5. These results show that with the reduction in L_{mb}, the energy spacing between the two modes (PBS1 and PSB2) seen in this figure increases [Figs. 5(a) and 5(a′)]. In this figure we also see the corresponding squared amplitudes of longitudinal mode profiles of each photonic subbands ($|F^I_{\omega_c}+R^I_{\omega_c}|^2$). In contrast to Fig. 4, here the mode profiles tend to be symmetric. The asymmetries seen here are caused by numerical uncertainties in finding the frequency of the modes. In fact because of the large confinement the widths of these modes are very small. Therefore, their exact wavelength search requires very small interval in the data files. The results shown in Fig. 5 indicate that as L_{mb} is decreased the shorter wavelength mode tends to become a single peak. In fact when $L_{\mathrm{bm}}=0$ we have a single photonic QW structure,

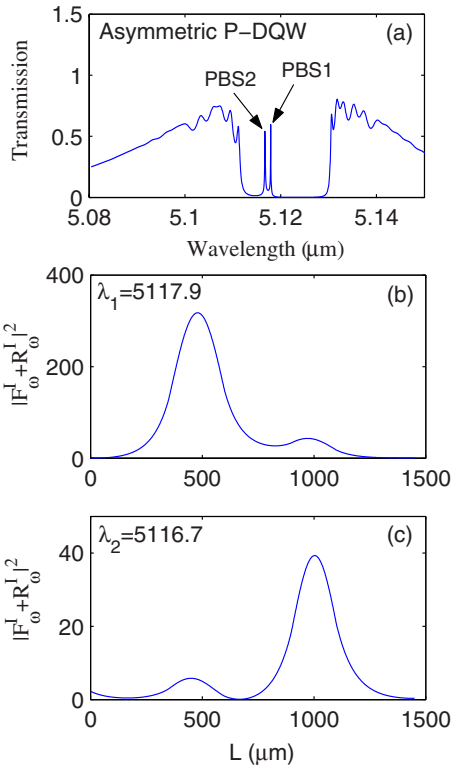

FIG. 4. (Color online) (a) Transmission of the waveguide structure shown in Fig. 1. The intensity and wavelength of the control laser are considered to be the same as those in Fig. 3. Here $L_{\mathrm{w1}}=250$, $L_{\mathrm{w2}}=200$ μm, and the thickness of the middle barrier (L_{mb}) is 300 μm. (b) and (c) show the squares of the longitudinal profiles of the modes at 5117.9 nm (PBS1) and 5116.7 nm (PBS2).

wherein the upper energy mode remains a doublet while the lower energy one becomes a single peak.[14] These features are very similar to standard symmetric single semiconductor QW structures.

To see the bonding and antibonding nature of the modes in Fig. 5, in Fig. 6 inset we show the real parts of $F^I_{\omega}+R^I_{\omega}$ for PSB1 (dashed line) and PSB2 (solid line) when $L_{\mathrm{mb}}=300$ μm. For the lower energy subband (PSB1) we can see $\mathrm{Re}[F^I_{\omega_c}+R^I_{\omega_c}]$ is more or less symmetric while that of the higher subband (PSB2) is antisymmetric.

To further investigate bonding and antibonding nature of PSB1 and PSB2, in Fig. 6 we show the overall variation in the wavelengths of these two photonic subbands in the symmetric P-DQW as L_{mb} is varied. Here we considered $L_{\mathrm{w1}}=L_{\mathrm{w2}}=200$ μm. As can be seen here, as L_{bm} decreases the two subbands are pushed away from each other. This has significant similarities with the bonding and antibonding states in symmetric S-DQWs and photonic molecules. The latter was demonstrated by fabricating pairs of micrometer-sized semiconductor cavities connected together via a narrow channel[7] or evanescent electromagnetic field.[17–19] By reducing the length of the channel it was shown that the energy splitting of the confined photonic modes increases, in close analogy with the emergence of electronic bonding and antibonding states in diatomic molecules. In this paper, however, by changing the illumination length of the middle barrier we adjust the strength of coupling between the photonic QWs.

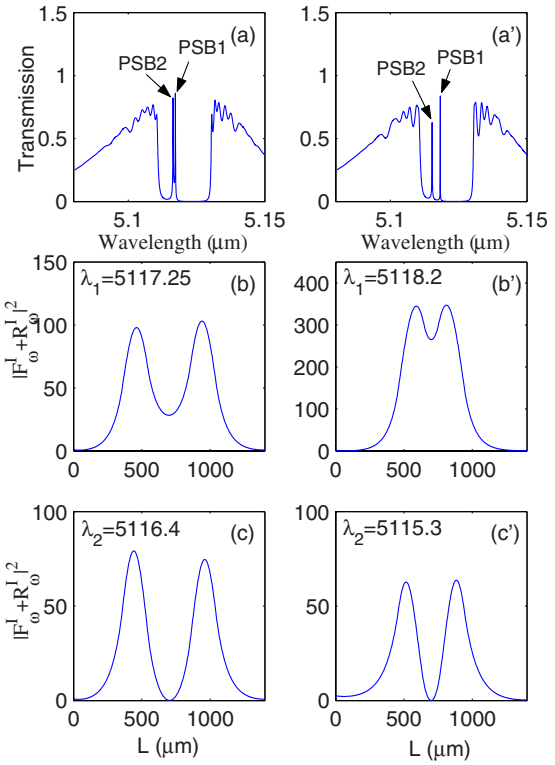

FIG. 5. (Color online) Similar to Fig. 4 but now $L_{w1}=200$, $L_{w2}=200$, and [(a)–(c)] $L_{mb}=300$ μm or [(a′)–(c′)] 100 μm. Numbers in legends show the wavelength of each mode in nanometer.

This allows us to control the strength of bonding and antibonding photonic modes and their energies.

Note that the P-DQW proposed in this paper was obtained by enhancing the contrast of refractive index perturbations in specific regions of a waveguide structure using coherent effects. These regions then acted as photonic barriers, causing confinement of photons and formation of photonic modes. The overall physics behind this phenomenon can be related to the fact that in the absence of the control field, the QW regions of the waveguide had lower refractive indices than those of the semiconductors in the trenches. Therefore, coherent suppression of refractive index in these regions caused further increase in the index contrast. Because of simultaneous generation of EIT, this process happened without generation of any significant loss. Formation of photonic modes or subbands in the P-DQW can, therefore, be related to scattering of electromagnetic waves from the illuminated and unilluminated regions, which effectively form two photonic wells coupled to each other. Such photonic modes were very similar to the conduction subbands of S-DQWs. However, if one designs the waveguide structure such that QW regions have higher refractive indices than those of the trenches, with the application of coherent enhancement of refractive index we can generate photonic modes very similar to the valence subbands of S-DQWs.[13]

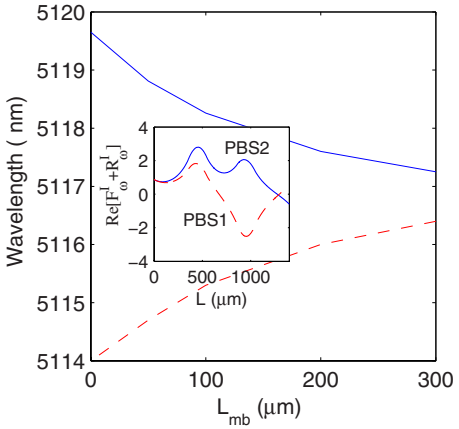

FIG. 6. (Color online) Variation in the wavelength of the photonic subbands in the P-DQW when L_{mb} is changed. Here $L_{w1}=L_{w2}=200$ μm. All other specifications are the same as those in Fig. 5. Inset show real parts of $(F^I_\omega+R^I_\omega)$ for PSB2 ($\lambda_1=5117.2$ nm) and PBS1 ($\lambda_2=5116.4$ nm). All other specifications are the same as those in Fig. 5.

In conclusion, we studied generation of photonic modes, including bonding and antibonding modes, in photonic double quantum well formed via interaction of a laser field with a semiconductor waveguide. This waveguide could form photonic heterostructures when a part of it was illuminated with a laser field, generating coherently controlled optical processes in that region. These processes included electromagnetically induced transparency and coherent suppression of refractive index. We showed that by changing the illumination geometry, one could change the parameters of the photonic double quantum well dynamically, going from a uniform passive PBG to the case where photonic bonding and antibonding modes or pure photonic subbands are formed. We showed that such a photonic quantum well presented significant one-to-one correspondence with type I electronic semiconductor double quantum wells.

*seyed.sadeghi@uah.edu

[1] J. P. Reithmaier, M. Rohner, H. Zull, F. Schafer, A. Forchel, P. A. Knipp, and T. L. Reinecke, Phys. Rev. Lett. **78**, 378 (1997).

[2] S. Chen, B. Qian, K. Chen, X. Zhang, J. Xu, Z. Ma, W. Li, and X. Huang, Appl. Phys. Lett. **90**, 174101 (2007).

[3] A. Verger, C. Ciuti, and I. Carusotto, Phys. Rev. B **73**, 193306 (2006).

[4] F. M. Weber, M. Karl, J. Lupaca-Schomber, W. Löffler, S. Li, T. Passow, J. Hawecker, D. Gerthsen, H. Kalt, and M. Hetterich, Appl. Phys. Lett. **90**, 161104 (2007).

[5] G. Schedelbeck, W. Wegscheider, M. Bichler, and G. Abstreiter, Science **278**, 1792 (1997).

[6] U. Banin, Y. W. Cao, D. Katz, and O. Millo, Nature (London) **400**, 542 (1999).

[7] M. Bayer, T. Gutbrod, J. P. Reithmaier, A. Forchel, T. L. Reinecke, P. A. Knipp, A. A. Dremin, and V. D. Kulakovskii, Phys.

Rev. Lett. **81**, 2582 (1998).
[8] M. Bayer, T. Gutbrod, A. Forchel, P. A. Knipp, and T. L. Reinecke, Phys. Status Solidi A **178**, 545 (2000).
[9] T. Gutbrod, M. Bayer, A. Forchel, P. A. Knipp, T. L. Reinecke, A. Tartakovskii, V. D. Kulakovskii, N. A. Gippius, and S. G. Tikhodeev, Phys. Rev. B **59**, 2223 (1999).
[10] M. Benyoucef, S. Kiravittaya, Y. F. Mei, A. Rastelli, and O. G. Schmidt, Phys. Rev. B **77**, 035108 (2008).
[11] J. Zi, J. Wan, and C. Zhang, Appl. Phys. Lett. **73**, 2084 (1998).
[12] Y. Jiang, C. Niu, and D. L. Lin, Phys. Rev. B **59**, 9981 (1999).
[13] S. M. Sadeghi, W. Li, X. Li, and W.-P. Huang, Phys. Rev. B **77**, 125313 (2008).
[14] S. M. Sadeghi and W. Li, Phys. Rev. B **80**, 045316 (2009).
[15] M. O. Scully and M. S. Zubairy, *Quantum Optics* (Cambridge University Press, Cambridge, England, 1997).
[16] S. M. Sadeghi, X. Li, W.-P. Huang, and W. Li, J. Appl. Phys. **101**, 123107 (2007).
[17] X. Li, R. C. Myers, F. M. Mendoza, D. D. Awschalom, and N. Samarth, IEEE J. Quantum Electron. **45**, 932 (2009).
[18] T. Mukaiyama, K. Takeda, H. Miyazaki, Y. Jimba, and M. Kuwata-Gonokami, Phys. Rev. Lett. **82**, 4623 (1999).
[19] M. D. Barnes, S. M. Mahurin, A. Mehta, B. G. Sumpter, and D. W. Noid, Phys. Rev. Lett. **88**, 015508 (2001).